# Simplified Mechanistic Model for Seismic Response Prediction of Coupled Cross-Laminated Timber Rocking Walls

Z. Jin[1]; S. Pei[2]; H. Blomgren[3]; and J. Powers[4]

**Abstract:** A simplified mechanistic model is developed in this study to predict the lateral load resistance of coupled rocking walls made from cross-laminated timber (CLT) panels as an alternative to finite-element modeling. The model is derived in an incremental format in order to capture the nonlinear behavior of the rocking wall, including crushing of the corners and inelastic response of interpanel connectors. The backbone curve and limit states generated using the proposed model are verified through a detailed finite-element model. Following the validation of the backbone curve, a spectrum-based maximum displacement prediction method is proposed for the rocking wall system under an arbitrary earthquake input. This simplified prediction method is validated using full-scale shake table test data of a two-story wood building with coupled CLT rocking walls. The model and the dynamic response prediction approach are found to be reasonably accurate for preliminary seismic design and evaluation of CLT rocking wall systems, so that detailed finite-element modeling and nonlinear time history analysis may not be necessary. **DOI: 10.1061/(ASCE)ST.1943-541X.0002265.** 



## Introduction

Cross-laminated timber (CLT) is an engineered wood panel product made from layers of lumber lamina glued together in an orthogonal pattern. There is a growing trend to construct multistory building using CLT as floor diaphragms and walls. A number of multistory CLT buildings have been built around the world with different structural configurations. Platform CLT buildings using CLT panels as both the floors and bearing walls are easy to construct, but have limited ductility unless long CLT panel shear walls are split into shorter segments with relatively high height:length ratios (Pei et al. 2013). Such buildings are typically built in regions with lower seismic demands (e.g., multistory CLT buildings in London and Melbourne). Another form of CLT building design combines CLT diaphragm with a traditional glulam column–beam system as gravity framing (e.g., the Wood Design and Innovation Center in Canada, the Carbon 12 Building in Portland, Oregon, and the Brock Commons Building at the University of British Columbia). Such a design requires separate lateral force-resisting systems that are typically balloon-framed into the wood-based gravity system. Because seismic design provisions for CLT lateral systems have not been well-established in current building codes in North America, a few existing tall CLT buildings used steel or concrete lateral systems that are recognized in current codes. There is currently no standard CLT-based lateral force-resisting solution for multistory wood buildings, especially in regions with high seismicity.

Rocking wall (or frame) systems have been studied in the past by the concrete and steel research communities (e.g., Wada et al. 2010; Andrea et al. 2014; Deierlein et al. 2011). Existing research findings indicated that rocking wall systems can be designed to achieve low damage during small to moderate earthquakes and be easily repairable after large earthquakes. Wood-based rocking wall systems have also been tested, and were used first in New Zealand (Smith et al. 2007; Loo et al. 2014) and later in the United States (Ganey et al. 2017; Akbas et al. 2017). With the reduced seismic mass of a wood building and the inherent flexibility of wood material, mass timber buildings with CLT rocking walls and wood gravity-frame systems can achieve very high-resilience performance. This was demonstrated in a series of full-scale shake table tests on a two-story CLT building as part of the Natural Hazards Engineering Research Infrastructure Program (NHERI) Tall Wood Project (Pei et al. 2017). One of the configurations tested in this program, a pair of coupled CLT rocking walls designed by Katerra (Seattle, Washington), was installed and subjected to 13 seismic tests (Fig. 1). The test results verified the ability of the rocking wall design to remain elastic when subjected to service-level earthquakes and to adequately control building drift when subjected to larger earthquakes. These tests also provided a great set of full-scale test data to validate the rocking wall model and displacement prediction method proposed here.

This study presents a mechanistic model used to predict the lateral pushover behavior of coupled CLT rocking wall systems (to obtain the backbone curve of the rocking wall). In order to facilitate displacement-based design of the rocking wall systems, this model is combined with a spectrum-based displacement prediction approach to estimate the maximum building dynamic response under a given ground motion input. Although nonlinear finite-element (FE) models (FEMs) and time history simulation can be employed for the same purpose, it is believed that a simpler mechanistic model for coupled rocking wall system can be of great value for preliminary performance prediction and design. The following sections present the analytical pushover process to derive the theoretical backbone curve for the rocking wall system. The analytical solution is compared with finite-element simulation and validated. Then the simplified approach to predict rocking wall

[1]Associate Professor, School of Civil Engineering, Southwest Jiaotong Univ., Chengdu 610031, China.

[2]Assistant Professor, Dept. Civil and Environmental Engineering, Colorado School of Mines, Golden, CO 80401 (corresponding author). Email: spei@mines.edu

[3]Director of Testing and Characterization, Katerra, Seattle, WA 98101.

[4]Engineer Associate, Katerra, Seattle, WA 98101.

Note. This manuscript was submitted on November 29, 2017; approved on August 16, 2018No Epub Date. Discussion period open until 0, 0; separate discussions must be submitted for individual papers. This paper is part of the ***Journal of Structural Engineering***, © ASCE, ISSN 0733-9445.

**Fig. 1.** Full-scale wood building with coupled rocking CLT walls designed by Katerra. (Image by S. Pei.)

peak dynamic response under earthquake excitation is proposed and validated through comparison with full-scale shake table test results.

## Coupled CLT Rocking Wall System

A coupled rocking wall configuration is commonly used in rocking wall design because it allows additional energy dissipation through connectors between rocking wall panels. Although there can be more than two rocking panels in a coupled wall series, a two-panel coupled rocking wall captures the kinematics of the system and is the configuration that was tested most in past research work (Ganey et al. 2017). Moreover, because the analytical model proposed here was validated with full-scale shake table test data from a building with two-panel coupled wall system, the discussion in this study is focused on two-panel coupled rocking wall configuration.

A coupled wall consists of two identical panels placed next to each other on a rigid foundation. The two panels are linked by a series of shear connectors at their interface (i.e., coupling elements). The shear connectors can be designed to remain elastic at the service load level in order to improve the lateral stiffness of the coupled wall. The connectors will also yield under larger earthquakes to help dissipate dynamic energy. The corners of the rocking wall panels are referred to here as the toes of the rocking wall. The rocking wall considered in this study also has hold-down elements placed at the center of the panel width to resist overturning. These hold-down elements can be simple mechanical connections that prevent the wall from uplifting, or posttensioned rod elements. The configuration of the rocking wall is illustrated in Fig. 2.

The coupling shear connectors are typically made of steel with the intention of yielding behavior for energy dissipation. Design options for these connectors may vary depending on construction details (e.g., water-jetted steel plates or U-shaped steel connectors), but the shear behavior of these connectors can typically be idealized as elastoplastic. In posttensioned rocking wall cases, the hold-down connector spring is posttensioned and remains elastic under design level loads. Thus it can be idealized as a linear spring. If other forms of hold-down elements are used, it can be assumed that the hold-downs are metal connectors that can exhibit a plastic yielding behavior when force demands become high.

Under lateral loads, the toe of each CLT panel bears on the foundation and may be crushed. There are different design options for the toe detail, including strengthening the toe to prevent damage or

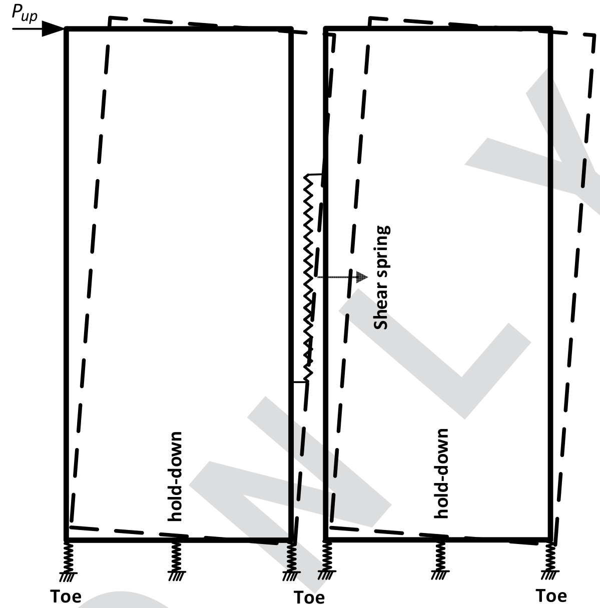


**Fig. 2.** Simplified kinematics configuration of coupled CLT rocking wall.

allowing the toe to be damaged for additional energy dissipation. Specifically, CLT toes experience strain hardening as the wood material densifies during the process of crushing. Thus it is logical to model the toe with a bilinear spring element with a postyielding stiffness. In summary, a generalized coupled CLT rocking wall model will include a number of key parameters listed in the Appendix. These parameters serve as the input for the proposed mechanistic model and dictate the behavior of the rocking wall under lateral load. Using this model, a designer will be able to quickly identify different limit states of various rocking wall designs, such as panel decompression, toe yielding/crushing, interpanel connector yielding, and hold-down yielding, without constructing nonlinear finite-element models.

## Mechanistic Model of Coupled Wood Rocking Wall System

Depending on the strength and stiffness of the connectors (hold-downs or shear connectors) relative to that of the toe of the panel, the rocking wall system can behave differently. This derivation numerically pushes the top of a coupled rocking wall incrementally and seeks to establish force equilibrium under a set of simple kinematics assumptions. Once the lateral force is determined through equilibrium at every incremental step, the pushover backbone curve of the wall is obtained. This derivation assumes that the amount of rotation of both panels stays the same throughout the pushover. Secondly, the total lateral pushing force equals the sum of the resultant lateral forces from the tops of both panels. Given these conditions, it is possible for the rocking wall to experience five distinct loading phases, which are described subsequently.

### *Phase 1: From Zero Lateral Load to Decompression*

Decompression happens when the lateral force grows large enough to balance the gravity load and the posttension force on the wall panels. The forces applied on the two panels at the point of decompression can be calculated as shown in Fig. 3.

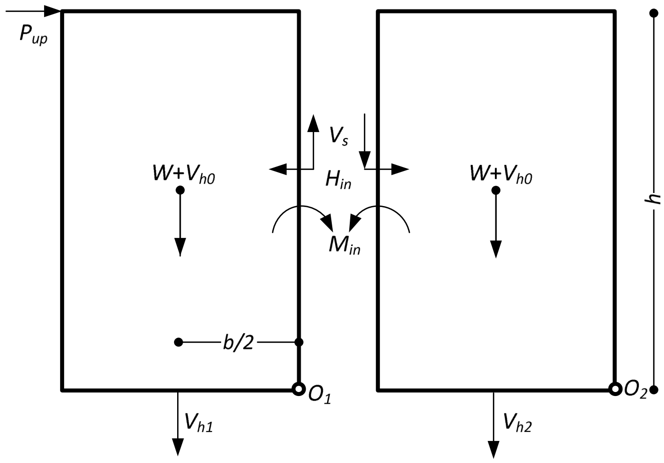


**Fig. 3.** Forces acting on panels at decompression load.

The moment equilibrium of the two panels about $O_1$ and $O_2$ requires

$$P_{\text{up}}h + M_{\text{in}} - H_{\text{in}} \cdot h/2 - (W + V_{h0} + V_{h1}) \cdot b/2 = 0 \quad (1)$$

$$-M_{\text{in}} + H_{\text{in}} \cdot h/2 - V_s \cdot b - (W + V_{h0} + V_{h2}) \cdot b/2 = 0 \quad (2)$$

where $W$ = self-weight of the wall; $V_{h0}$ = prestressing force in the hold-down bar; and $V_{h1}$ and $V_{h2}$ = incremental hold-down forces caused by panel rotation. Because the rotation angle $\alpha$ is very small at decompression, the coupling shear force $V_s$ and the incremental hold-down forces $V_{h1}$ and $V_{h2}$ can be neglected. Adding Eqs. (1) and (2) obtains

$$P_{\text{up}} = (W + V_{h0}) \cdot b/h \quad (3)$$

As the lateral force increases, the vertical load on the left toe shifts to the right toe gradually. The initial compression deformation of the toe spring is $(W + V_{h0})/(2K_{t0})$, and thus the rotation angle leading to decompression of the left toe is $\alpha_{\text{up}} = (W + V_{h0})/(2K_{t0})/(b/2)$. Therefore, the lateral displacement at the top can be calculated as

$$U_{\text{up}} = \alpha_{\text{up}}h = (W + V_{h0})h/K_{t0}/b \quad (4)$$

At this point, the force in the toes at both panels are the same

$$V_{t1,\text{up}} = W + V_{h0} \quad (5)$$

The elastic displacement of the wall top is $U_{e,\text{up}} = P_{\text{up}}h^3/(3EI)$, where $I = 2tb^3/12$ (the bending moment of inertia of the coupled wall cross section), and $E$ and $t$ are the equivalent elastic modulus and the thickness of the wall panel, respectively. Thus, the shear spring force from the elastic bending deformation of the wall is

$$V_{s,\text{up}} = 2K_s(W + V_{h0})h/b/(Et) \quad (6)$$

where $K_s$ = stiffness of the shear spring. If the rocking wall system is posttensioned, or has very large vertical loading (load bearing wall), it is possible in theory to yield the toe or shear spring before decompression happens. However, for typical rocking wall design, decompression is typically the first limit stage encountered under increasing lateral loads.

### *Phase 2: From Decompression to Yielding of Shear Spring*

Theoretically, it is possible to crush the toe before the yielding of shear spring if the toe is relatively weak. However, the main purpose of shear elements in realistic designs is to help dissipate energy, thus the coupling elements are typically designed to yield first in most cases. After decompression, the compression forces on the wall panels are resisted by the toes. The rotation of the panel continues as the hold-down spring elongates. Once the rotation exceeds a certain level, the interpanel shear connector yields. The lateral drift level at yielding mainly depends on the interpanel shear connector's yielding displacement and the panel aspect ratio. The incremental displacement and force relationship for the wall system during this phase is summarized as follows (Appendix I provides the detailed derivation).

The incremental lateral drift $\Delta U_{ys}$ can be calculated as

$$\Delta U_{ys} = h\Delta\alpha_{ys}, \quad \text{where } \Delta\alpha_{ys} = (F_s/b/K_s - \alpha_{\text{up}})[1 + 2K_s/(K_{t0} + K_h)] \quad (7)$$

where $\alpha_{\text{up}} = U_{\text{up}}/h$ = nominal rotation at decompression.

The incremental lateral force is

$$\Delta P_{ys} = \frac{K_h K_{t0}}{K_h + K_{t0}}\Delta\alpha_{ys} \cdot b^2/h/2 + [F_s - K_s b\alpha_{\text{up}}]b/h \quad (8)$$

The incremental forces in the hold-down and at the toes can be calculated by

$$\Delta V_{h1,ys} = e_1 K_h \Delta\alpha_{ys}, \quad \Delta V_{h2,ys} = e_2 K_h \Delta\alpha_{ys} \quad (9)$$

$$\Delta V_{t1,ys} = (b/2 - e_1)K_{t0}\Delta\alpha_{ys}, \quad \Delta V_{t2,ys} = (b/2 - e_2)K_{t0}\Delta\alpha_{ys} \quad (10)$$

In Eqs. (9) and (10), $e_1$ and $e_2$ are the distances between the rotation center and the panel center at Phase 2

$$e_{1,2} = b\left(\frac{K_{t0}/2}{K_{t0} + K_h} \pm \frac{K_s}{K_{t0} + K_h + 2K_s}\right) \quad (11)$$

### *Phase 3: Yielding of Toe on Right Panel*

After the yielding of the shear spring, the shear force between panels remains constant. From the vertical equilibrium condition each panel, the sum of the incremental hold-down force and the toe force equals the incremental shear force, which is zero after yielding. Therefore, after the yielding of the shear spring, the panels will rotate in a specific way so that the incremental hold-down force always balances the incremental toe force. Based on this condition, the location of the rotation center can be calculated as

$$e'_{1,2}K_h = (b/2 - e'_{1,2})K_{t0}, \quad \text{or} \quad e'_{1,2} = \frac{b}{2}\frac{1}{(1 + K_h/K_{t0})} \quad (12)$$

The toe for the right panel (when the lateral load is applied from left to right) will always take a higher load than the toe of the left panel. Thus the right panel toe will yield first if the materials of both panels are the same.

Incremental force of the toe spring is

$$\Delta V_{t2,yt2} = (b/2 - e'_2)K_{t0}\Delta\alpha_{yt2} \quad (13)$$

The right panel toe will yield when

$$W + V_{h0} + \Delta V_{t2,ys} + \Delta V_{t2,yt2} = F_t \tag{14}$$

Thus, by substituting Eq. (14) into Eq. (13), the yielding of the right toe will happen when the incremental angle is

$$\Delta\alpha_{yt2} = \frac{F_t - W - V_{h0} - \Delta V_{t2,ys}}{(b/2 - e_2')K_t} \tag{15}$$

At this time, the incremental force on the left panel toe is

$$\Delta V_{t1,yt2} = (b/2 - e_1')K_{t0}\Delta\alpha_{yt2} \tag{16}$$

The incremental hold-down force can also be calculated based on geometry

$$\Delta V_{h1,yt2} = K_h e_1' \Delta\alpha_{yt2}, \quad \Delta V_{h2,yt2} = K_h e_2' \Delta\alpha_{yt2} \tag{17}$$

Finally, the incremental lateral force is

$$\Delta P_{yt2} = K_h \Delta\alpha_{yt2} \cdot (e_1' + e_2') b/h/2 \tag{18}$$

### Phase 4: Yielding of Left Panel Toe

Similar to Phase 3, before the yielding of the left panel toe, the left panel will continue to rotate about $e_1'$, and the incremental toe force at the yielding of the left panel toe can be written as

$$\Delta V_{t1,yt1} = \left(\frac{b}{2} - e_1'\right) K_{t0} \Delta\alpha_{yt1} \tag{19}$$

The left toe will eventually yield as the rotation continues to increase

$$W + V_{h0} + \Delta V_{t1,ys} + \Delta V_{t1,yt1} + \Delta V_{t1,yt2} = F_t \tag{20}$$

From Eqs. (18) and (19), the incremental rotation angle as the left panel toe yields is

$$\Delta\alpha_{yt1} = \frac{F_t - (W + V_{t1,yt2} + \Delta V_{t1,ys})}{(b/2 - e_1')K_{t0}} \tag{21}$$

After the yielding of the right panel toe, the rotation center of the right panel shifts to

$$e_1'' = \frac{b}{2} \frac{1}{(1 + K_h/K_{t1})} \tag{22}$$

Eq. (22) is the result of replacing the initial stiffness $K_{t0}$ with the postyielding stiffness $K_{t1}$ in Eq. (12). The incremental hold-down force can be calculated as

$$\Delta V_{t1,yt1} = K_h e_1' \Delta\alpha_{yt1}, \Delta V_{h2,yt1} = K_h e_2'' \Delta\alpha_{yt1} \tag{23}$$

Similar to the right panel toe, the incremental toe force is

$$\Delta V_{t2,yt1} = (b/2 - e_2'')K_{t1}\Delta\alpha_{yt1} \tag{24}$$

The incremental lateral force can be calculated using a formula similar to Eq. (18), by replacing $e_2'$ with $e_2''$ and $\Delta\alpha_{yt1}$ with $\Delta\alpha_{yt2}$

$$\Delta P_{yt1} = K_h \Delta\alpha_{yt1} \cdot (e_1' + e_2'') \frac{b/h}{2} \tag{25}$$

### Phase 5: Yielding of Left Panel Hold-Down

After both panel toes yield, the toe force will continue to increase because the wood in compression is not elastoplastic. Eventually, it is possible for the hold-down to yield under large rotation. After the yielding of the both toes, the rotation center of both panels can be determined by [Eq. (22)]

$$e_{1,2}'' = \frac{b}{2} \frac{1}{(1 + K_h/K_{t1})} \tag{26}$$

Because the left hold-down spring takes more hold-down force than the right hold-down spring due to geometry, the left hold-down spring will yield first (assuming that the hold-down systems in both panels are the same). The left hold-down spring yields when

$$\Delta\alpha_{yh1} e_1'' + D_{h1,yt1} = F_h/K_h, \quad \text{where } D_{h1,yt1} = \Delta\alpha_{yt1} e_1' + \Delta\alpha_{yt2} e_1' + \Delta\alpha_{ys} e_1 \tag{27}$$

From Eq. (27), the incremental rotation angle $\Delta\alpha_{yh1}$ can be solved. At this moment, the hold-down force increment on the right panel can be written

$$\Delta V_{h2,yh1} = K_h e_2'' \Delta\alpha_{yh1} \tag{28}$$

The incremental toe forces are

$$\Delta V_{t1,yh1} = (b/2 - e_1'')K_{t1}\Delta\alpha_{yh1}, \quad \Delta V_{t2,yh1} = (b/2 - e_2'')K_{t1}\Delta\alpha_{yh1} \tag{29}$$

The lateral force increment at the left hold-down spring yielding is

$$\Delta P_{yh1} = K_h \Delta\alpha_{yh1} \cdot (e_1'' + e_2'') \frac{b/h}{2} \tag{30}$$

### Phase 6: Yielding of Right Hold-Down

After the left hold-down spring yields, if the panel continues to rotate, the right hold-down will eventually yield. Beyond this stage, the rocking wall system will yield laterally and there will be no mechanism to generate additional resistance. After the left hold-down yields, the left panel rotates about its right corner; because the shear and hold-down springs both yield, no additional force can be generated to further compress the toe). The right panel center of rotation locates $e_2''$ from the panel center, as described for Phase 5.

The right hold-down spring yield when

$$\Delta\alpha_{yh2} e_2'' + D_{h2,yh1} = F_h/K_h, \quad \text{where } D_{h2,yh1} = \Delta\alpha_{yh1} e_2'' + \Delta\alpha_{yt1} e_2'' + \Delta\alpha_{yt2} e_2' + \Delta\alpha_{ys} e_2 \tag{31}$$

From Eq. (31), the incremental rotation angle $\Delta\alpha_{yh2}$ when the right hold-down spring yields can be solved. The incremental toe forces are

$$\Delta V_{t1,yh2} = 0, \qquad \Delta V_{t2,yh2} = (b/2 - e_2'')K_{t1}\Delta\alpha_{yh2} \tag{32}$$

The lateral force after the left hold-down spring yields is

$$\Delta P_{yh2} = K_h \Delta\alpha_{yh2} \cdot (b/2 + e_2'') \frac{b/h}{2} \tag{33}$$

Eq. (33) is the result of replacing $e_1''$ with $b/2$ in Eq. (30).

These six stages of possible coupled rocking wall behavior and their corresponding rotation and resistance calculations can be summarized in a set of limit states formulas (Appendix II). This analytical solution is presented in incremental format (except for Stage 1, given as the limits for this linear deformation stage) because the rocking wall connection elements (hold-down, toe, and shear connector) are nonlinear. The incremental formula can be implemented using Excel or another simple numerical program. For a particular wall design, with the properties of the shear, toe, and hold-down springs determined, the formula can be used to calculate the wall response under a monotonic pushover protocol (i.e., generating a backbone curve). These limit states can be identified along the backbone curve.

### Comparison of Analytical Backbone Curve and FEM Simulation

The analytical backbone curve derived in this study was compared with a nonlinear finite element model constructed using SAP2000 software (Computers and Structures Inc 2006) in order to illustrate the equivalency in these two approaches. Two rocking wall configurations were simulated based on realistic mass timber rocking walls configurations used in the aforementioned testing program. The first configuration was a rocking wall with very strong hold-down elements but no posttensioning. The second configuration was a modified version of the first, with posttensioning added and the hold-down/shear stiffness reduced. The design parameters for both cases are listed in Table 1.

The backbone curves of the wall obtained from the analytical solution and the FEM analysis are compared in Fig. 4. The analytical formula can accurately capture the overall trend of the backbone compared with FEM simulation. Furthermore, the rocking wall characteristics are very sensitive to the design parameters. There is a small discrepancy between the backbone curve from the analytical solution and the FEM which is induced by the elastic deformation of the wall panel, which was not considered in the simplified model (analytical derivation assumed the panels to be rigid). If desired, the elastic deformation can be calculated by $2P/E/t(h/b)^3$ and added to the total lateral deformation. Fig. 4 also shows the analytical backbone curve with the elastic deformation of the wall added. After considering the elastic deformation, the analytical solution is almost identical to FEM simulation result. In the following sections, the backbone curves used in the examples do not include the elastic deformation impact because (1) from Fig. 4, the elastic deformation is relatively small, and (2) in most practical cases, the lateral force is applied along the height of the wall at each floor and the roof, making the elastic deformation contribution even smaller compared with the case in which all lateral forces are applied on the roof.

## Seismic Response Prediction

Rocking wall system dynamic response is nonlinear under large earthquakes. Traditionally, nonlinear time history analysis needs to be conducted in order to estimate the dynamic displacement of the system. This process is time-consuming and requires significant efforts in modeling, making it difficult for preliminary design and assessment. For displacement-based design, the full time history of the wall response is typically not required. Design can be

**Table 1.** Example rocking wall parameters

| Symbol | Meaning | Case 1 | Case 2 | Unit |
|---|---|---|---|---|
| $E$ | Modulus of elasticity of wall material | $1.103 \times 10^{10}$ | $1.103 \times 10^{10}$ | N/m$^2$ |
| $b$ | Width of single panel | 1.524 | 1.524 | m |
| $t$ | Thickness of panel | 0.175 | 0.175 | m |
| $W$ | Self-weight of single panel | 915.3 | 915.3 | Kg |
| $V_{h0}$ | Prestressing force of hold-down | 0 | 10,000 | N |
| $K_h$ | Stiffness of hold-down tendon | $4.901 \times 10^8$ | $5.000 \times 10^6$ | N/m |
| $K_s$ | Stiffness of shear spring | $1.911 \times 10^7$ | $9.555 \times 10^6$ | N/m |
| $K_{t0}$ | Initial stiffness of toe spring | $2.942 \times 10^7$ | $2.942 \times 10^7$ | N/m |
| $K_{t1}$ | Toe spring stiffness after yielding | $8.262 \times 10^5$ | $8.262 \times 10^5$ | N/m |
| $F_s$ | Yielding force of shear spring | $9.710 \times 10^4$ | $9.710 \times 10^4$ | N |
| $F_t$ | Yielding force of toe spring | $1.644 \times 10^5$ | $1.644 \times 10^5$ | N |

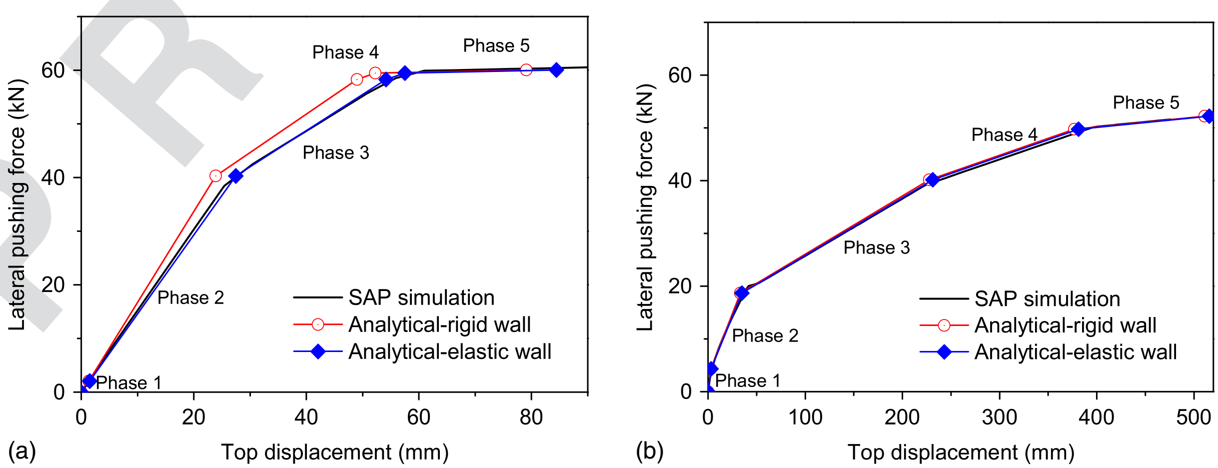


**Fig. 4.** Backbone curve of the rocking wall: (a) Case 1; and (b) Case 2.

conducted with an accurate estimation of the maximum displacement response. Therefore this paper proposes a simplified approach to calculate the maximum seismic response of the rocking wall against a given ground motion. This approach requires only the response spectrum of the ground motion and the analytical backbone curve derived previously (which can be obtained given basic design parameters of the wall). The method was applied to a coupled CLT rocking wall subjected to a series of earthquake excitations. The maximum displacement estimation was compared with full-scale shake table test results and showed satisfactory accuracy.

## Dynamic Equation for Rocking Wall System

The dynamic response of the rocking wall subjected to earthquake ground motion excitation can be written as a single-degree-of-freedom (SDOF) system in terms of the rotation angle

$$M_\alpha \ddot{\alpha} + C\dot{\alpha} + K_\alpha(\alpha)\alpha = -La(t) \quad \text{or}$$
$$\ddot{\alpha} + 2\varepsilon\omega_0\dot{\alpha} + \omega_0^2\alpha = -L/M_\alpha a_g(t) \tag{34}$$

where $M_\alpha = m_1 h_1^2 + m_2 h_2^2$ = mass moment of inertia of the building about the toe; and $L = m_1 h_1 + m_2 h_2$ = rotation moment factor from the ground motion excitation. This study used the NHERI Tall Wood two-story test building as an example, which has concentrated mass at the roof and floor levels. The secant stiffness of the wall $K_\alpha(\alpha)$ in rotation motion can be obtained by the backbone curve of the wall (example calculation is shown in section [10] "Simplified Approach for Displacement Prediction").

The rotation stiffness in Eq. (34) can be calculated by

$$K_\alpha(\alpha) = \frac{ph_2}{\alpha} = \frac{ph_2}{u/h_2} = \frac{P}{u}h_2^2 \tag{35}$$

where $P/u$ = secant stiffness from the backbone curve (Fig. 7).

## Simplified Approach for Displacement Prediction

We propose a graphic spectrum approach to estimate the drift of the rocking wall in the preliminary design stage. This approach avoids complicated FEM modeling and time-history simulations. Based on the linearization approach for random vibration theory, Eq. (34) can be linearized as

$$M_\varphi \ddot{\alpha} + C\dot{\alpha} + \bar{K}_\alpha \alpha = -La(t) \tag{36}$$

In Eq. (36), only the stiffness needs to be linearized. Assuming that the response distribution is Gaussian, the standard linearization approach (Caughey 1963) can be followed for dynamic system with Gaussian responses. The equivalent stiffness is calculated as

$$\bar{K}_\alpha(\sigma_\alpha) = E[K_\alpha(\alpha)] = \frac{1}{\sigma_\alpha\sqrt{2\pi}}\int_{-\infty}^{+\infty} K_\alpha(\alpha)\exp\left(-\frac{\alpha^2}{2\sigma_\alpha^2}\right)d\alpha \tag{37}$$

where $\sigma_\alpha$ = standard derivation of the wall rotation angle. For a Gaussian process the standard derivation can be approximated as one-third of the maximum value, that is

$$\sigma_\alpha \approx \alpha_{\max}/3 \ \text{ with } \ \alpha_p = \max(|a(t)|)/3 \tag{38}$$

Given the maximum rotation $\alpha_{\max}$ of the wall, the equivalent stiffness $\bar{K}_\alpha$ can be calculated from the backbone curve using Eqs. (35) and (37). Then the natural period of the linearized wall can be easily related to the maximum rotation of the wall by

$$T(\alpha_{\max}) = 2\pi\sqrt{\bar{K}_\alpha(\alpha_{\max}/3)/M_\alpha} \tag{39}$$

On the other hand, once the natural period of the wall is known, the maximum rotation of the wall can be determined using the response spectrum as

$$\alpha_{\max} = RS_d(T) \tag{40}$$

Finally, the maximum rotation and equivalent natural period can be found as the solution to Eqs. (39) and (40). The solution can be determined graphically on the $T$–$\alpha_{\max}$ plots from Eqs. (39) and (40). The procedure of the proposed graphical approach is illustrated in Fig. 5 as a six-step process.

Step 1. Convert the rocking wall backbone curve to the secant stiffness curve;

Step 2. Calculate the equivalent stiffness of the wall from the secant stiffness curve using Eqs. (37) and (38);

Step 3. Plot the natural period of the linearized panel using the equivalent stiffness;

Step 4. Calculate the displacement response curve for given ground motion;

Step 5. Find the intersection of the curves in Step 3 and Step 4, resulting in the nonlinear solution; and

Step 6. Take average of the linear solution and the nonlinear solution.

Details of this process are demonstrated using examples in the following section.

## Example Prediction and Validation

This study used experimental data from full-scaled shake table tests of a coupled rocking wall to validate the proposed displacement prediction approach. The full-scale CLT wall tested is shown in Fig. 6. Because the wall was balloon-framed with the diaphragm, the roof and floor in Fig. 6 did not interrupt the continuity of the rocking wall panels.

The rocking wall was designed without posttensioning (Fig. 6). Instead, the toe detail was specially designed to allow crushing into a sacrificial wood crushing block that can be quickly replaced after an earthquake (if needed). The parameters used for the wall design were those of Design Case 1 in Table 1.

### Demonstrative Example: Prediction of Single Test

As an example to demonstrate the six-step process of the proposed method, prediction of the rocking wall responses subjected to the Imperial Valley ground motion record scale with peak ground

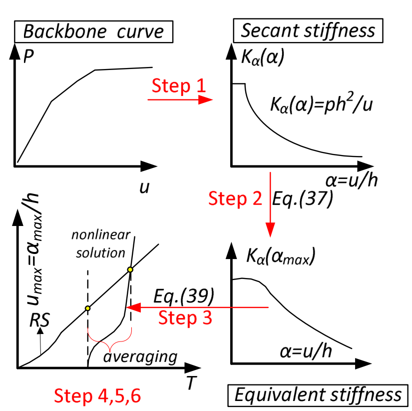


**Fig. 5.** Spectrum-based approach to estimate maximum wall displacement.

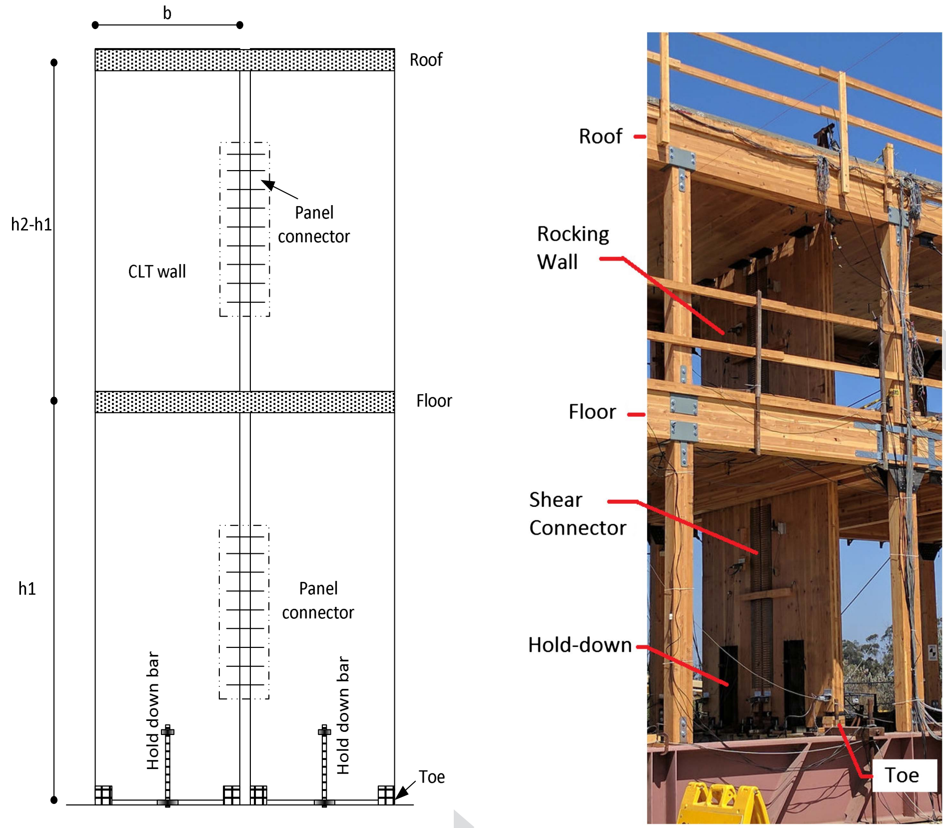


F6:1 **Fig. 6.** Detailed configuration of coupled CLT wall (designed by Katerra). (Image by S. Pei.)

acceleration (PGA) of 0.736g is illustrated here. The following steps were followed:

1. Convert the backbone curve ($P$–$u$ relation) in Fig. 4(a) into the secant stiffness curve in Fig. 7. Fig. 7 is related to Fig. 4(a) by the following conversion: rotation angle $\alpha = u/h$; and secant rotation stiffness $K_\alpha(\alpha) = (P/u)h^2$.
2. Calculate equivalent stiffness of the wall $[\bar{K}_\alpha(\sigma_\alpha)]$ from the secant stiffness in Fig. 7, using Eq. (37). Get the relation between the equivalent stiffness $\bar{K}_\alpha(\sigma_\alpha)$ and the maximum displacement $\alpha_{\max} = 3\sigma_\alpha$ (Fig. 8).
3. Get the dependence of equivalent period on the maximum displacement from Fig. 8 using $T(\alpha_{\max}) = 2\pi\sqrt{\bar{K}_\alpha(\sigma_\alpha)/M_\alpha}$, $\sigma_\alpha = \alpha_{\max}/3$, and $u_{\max} = h\alpha_{\max}$ (Fig. 9).
4. Calculate the displacement response spectrum of the wall. In Eq. (34), the ground motion should be scaled by $L/M_\alpha$ to obtain the response spectrum of the rotation angle.
5. Find the intersection of the two curves as the nonlinear solution.
6. Average the displacement between the linear and nonlinear responses on the response spectrum curve.

The estimated roof displacement based on the curve in Fig. 9 is 20.7 cm before averaging, and 28.1 cm after averaging.

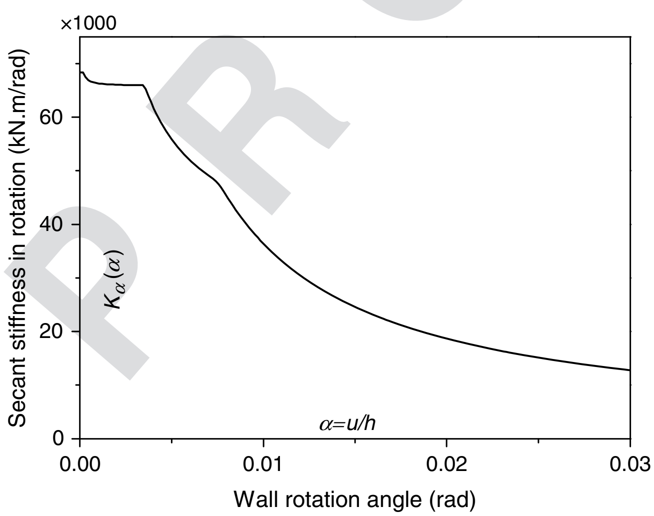


F7:1 **Fig. 7.** Secant stiffness versus wall rotation.

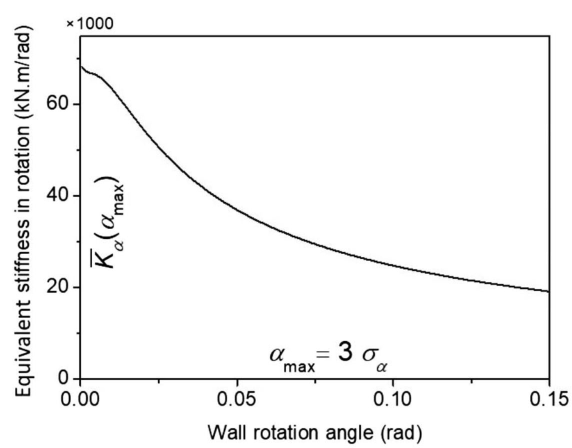


**Fig. 8.** Equivalent stiffness versus maximum wall rotation. F8:1

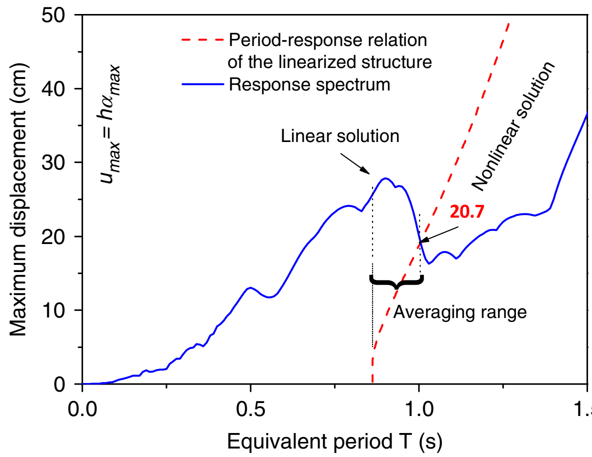


F9:1 **Fig. 9.** Graphical method to find maximum wall displacement.

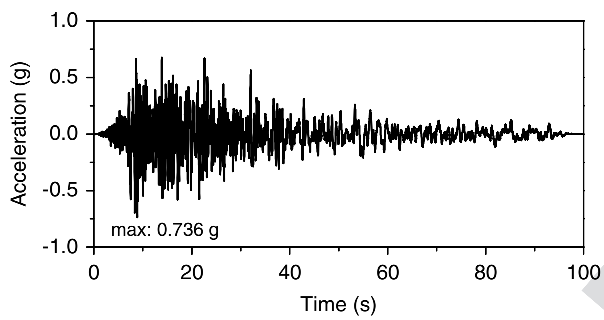


F10:1 **Fig. 10.** Ground motion record (Imperial Valley, with PGA = $0.736g$).

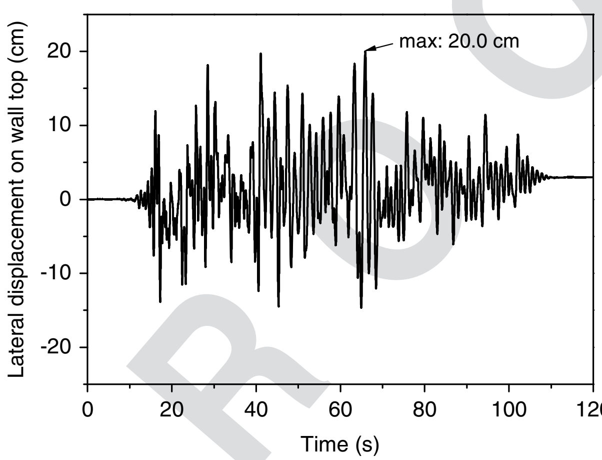


F11:1 **Fig. 11.** Measured roof displacement time history.

The purpose of averaging over the spectral response is to account for potential softening of the system during dynamic loading.

The ground motion acceleration time history and the roof displacement subjected to this ground motion are shown in Figs. 10 and 11. The measured maximum roof displacement is 20.0 cm, which is very close to the estimated response using the proposed method.

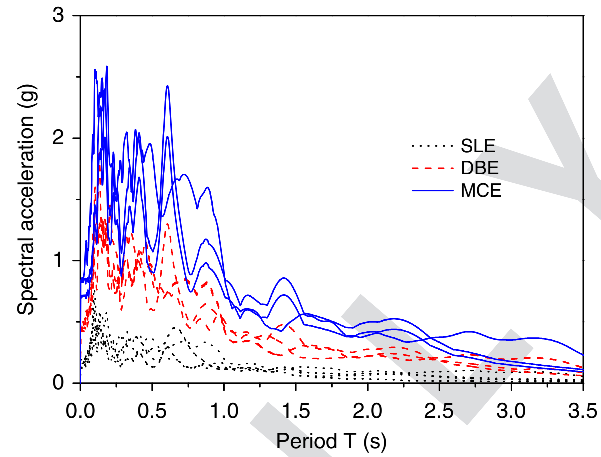


**Fig. 12.** Response spectrums of 13 tested ground motions. F12:1

**Validation Using Multiple Earthquakes**

Similar to the preceding process, all 13 cases of different GM records and PGA were predicted. The ground motions used in the test were scaled to three different intensity levels, namely the serviceability-level earthquake (SLE), design-basis earthquake (DBE), and maximum considered earthquake (MCE). The response spectrum of the ground motion records tested are shown in Fig. 12. During the 13 tests, a few variations of the interpanel shear connector configuration were tested. By applying different amounts (lengths) of interpanel steel connectors, the shear spring stiffness and strength changes. The lengths of the interpanel connector for the wall are listed in Table 2.

The estimated roof drift from the proposed methods are compared with the actual measurements in Fig. 13, with the relative error listed in Table 2. The comparison shows that the mean error of the proposed method is about 25%, with RMS of 12%–15% across all intensity levels. Considering the large uncertainty of ground motions, the accuracy of the proposed method can be accepted as a preliminary design tool.

## Conclusions

The lateral load-resisting behavior of a coupled rocking CLT wall system was investigated in this study. Analytical formulas that can be used to generate backbone curve of the coupled rocking wall were proposed. The model is able to represent different rocking wall design configurations given key load-resistance parameters for the toe, hold-down element, and interpanel shear connectors. The analytical backbone curves were compared with FEM simulation, validating the equivalency of the two methods.

Based on the backbone curve of the rocking wall, the equation of motion for a rocking wall system under seismic excitation was linearized, resulting in a simplified equivalent single-degree-of-freedom system. Then the maximum displacement of the rocking wall was estimated as the intersection point of the displacement response spectrum and the displacement–natural period curve (generated based on the nonlinear backbone curve). To further improve the accuracy of this graphic method, the spectrum averaging method was proposed in order to consider the nonlinear period elongation of the rocking walls. The proposed maximum displacement prediction method was compared with the results from full-scale system-level shake table tests. The accuracy of the proposed method was found to be reasonable for preliminary design and evaluation of CLT rocking walls.

**Table 2.** Ground motion records, shear connector length, and predicted drift errors for tests

| Test | Ground motion | Ground motion level | PGA ($g$) | Panel connector length [m (ft)] | Relative error of predicted roof drifts (%): Equivalent linearization, Individual analysis | Relative error of predicted roof drifts (%): Equivalent linearization, Average of intensity level | Relative error of predicted roof drifts (%): Average over spectrum, Individual analysis | Relative error of predicted roof drifts (%): Average over spectrum, Average of intensity level |
|---|---|---|---|---|---|---|---|---|
| 1 | Loma Prieta | SLE | 0.163 | 9.75 (32) | 15 | 23 | 15 | 21 |
| 2 | Superstition Hills | SLE | 0.154 | 9.75 (32) | 36 | | 30 | |
| 3 | Northridge | SLE | 0.134 | 4.88 (16) | 16 | | 19 | |
| 4 | Northridge | SLE | 0.115 | 9.75 (32) | 42 | | 36 | |
| 5 | Loma Prieta | SLE | 0.147 | 7.32 (24) | 13 | | 13 | |
| 6 | Imperial Valley | SLE | 0.190 | 9.75 (32) | 18 | | 15 | |
| 7 | Superstition Hills | DBE | 0.413 | 9.75 (32) | 8 | 31 | 15 | 34 |
| 8 | Imperial Valley | DBE | 0.395 | 4.88 (16) | 28 | | 50 | |
| 9 | Imperial Valley | DBE | 0.403 | 9.75 (32) | 60 | | 42 | |
| 10 | Northridge | DBE | 0.447 | 4.88 (16) | 29 | | 29 | |
| 11 | Imperial Valley | MCE | 0.813 | 7.32 (24) | 3 | 14 | 31 | 22 |
| 12 | Northridge | MCE | 0.697 | 7.32 (24) | 21 | | 21 | |
| 13 | Northridge | MCE | 0.821 | 7.32 (24) | 17 | | 14 | |

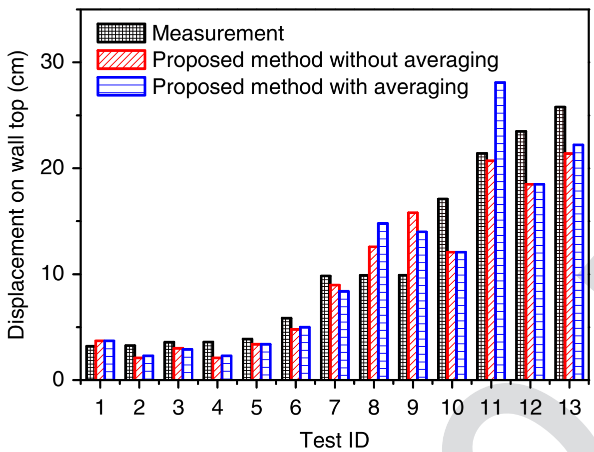


**Fig. 13.** Comparison of tested and estimated roof displacements.

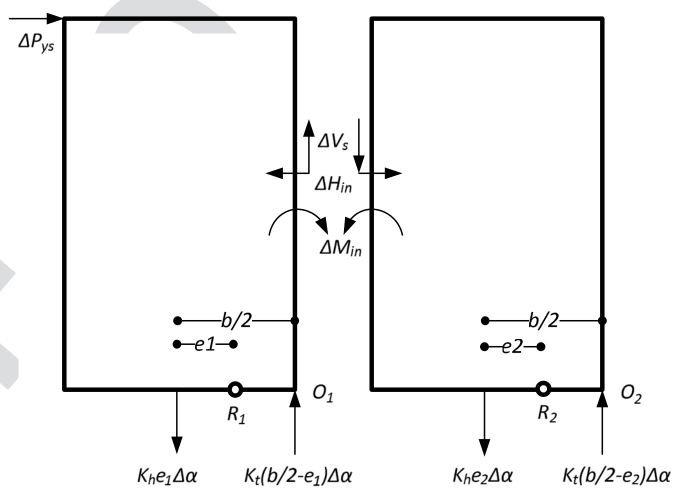


**Fig. 14.** Phase 2 panel equilibrium free body diagram.

## Appendix I. Detailed Derivation of Phase 2 Panel Equilibrium

The rotation centers of the panels in Phase 2 are marked $R_1$ and $R_2$ in Fig. 14, located $e_1$ and $e_2$ from the panel center.

As the panels rotate about $R_1$ and $R_2$ with an incremental rotation angle $\Delta\alpha$, the incremental hold-down forces and toe forces can be calculated by the spring elongation as shown in Fig. 14. The incremental hold-down forces are $K_h e_1 \Delta\alpha$ (left panel) and $K_h e_2 \Delta\alpha$ (right panel), and the incremental toe forces are $K_t(b/2 - e_1)$ (left panel) and $K_t(b/2 - e_2)$ (right panel).

The vertical equilibriums (incremental form) of the left and the right panels are

$$\Delta V_s + K_{t0}(b/2 - e_1)\Delta\alpha - K_h e_1 \Delta\alpha = 0 \quad (41)$$

$$-\Delta V_s + K_{t0}(b/2 - e_2)\Delta\alpha - K_h e_2 \Delta\alpha = 0 \quad (42)$$

The rotation center $e_1$ and $e_2$ can be solved using the equilibrium Eqs. (41) and (42) as

$$e_1 = (\Delta V_s/\Delta\alpha + K_{t0} b/2)(K_h + K_{t0}) \quad (43)$$

$$e_2 = (-\Delta V_s/\Delta\alpha + K_{t0} b/2)(K_h + K_{t0}) \quad (44)$$

The incremental shear force can be calculated according to the elongation of the shear spring by

$$\Delta V_s = K_s[(b/2 - e_1) + (b/2 + e_2)]\Delta\alpha = K_s(b + e_2 - e_1)\Delta\alpha \quad (45)$$

By substituting Eqs. (43) and (44) into Eq. (45), the incremental shear force can be solved as

$$\Delta V_s = \frac{K_s b \Delta\alpha}{1 + 2K_s/(K_{t0} + K_h)} \quad (46)$$

Then, by substituting Eq. (46) into Eq. (43) and Eq. (44), the rotation center location can be determined by

$$e_{1,2} = b\left[\pm\frac{K_s}{K_{t0} + K_h + 2K_s} + \frac{K_{t0}/2}{K_{t0} + K_h}\right] \quad (47)$$

The shear spring yields when

$$\Delta V_s + K_s b \alpha_{\mathrm{up}} = F_s \quad (48)$$

where $\alpha_{\mathrm{up}}$ = panel rotation at the decompression phase; and $F_{ys}$ = yielding strength of the shear spring. By substituting Eq. (48) into

Eq. (46), the incremental rotation angle and lateral displacement at the top when the shear spring yields can be found

$$\Delta\alpha_{ys} = [F_s/K_s/b - \alpha_{\text{up}}][1 + 2K_s/(K_{t0} + K_h)] \quad \text{and}$$
$$\Delta U_{ys} = h\Delta\alpha_{ys} \tag{49}$$

Given the incremental rotation angle $\Delta\alpha_{ys}$ in Eq. (49) and the rotation center $e_{1,2}$ in Eq. (47), the forces in the hold-down and at the toes can be calculated

$$\Delta V_{h1,ys} = e_1 K_h \Delta\alpha_{ys},$$
$$\Delta V_{h2,ys} = e_2 K_h \Delta\alpha_{ys} \tag{50}$$

$$\Delta V_{t1,ys} = (b/2 - e_1)K_{t0}\Delta\alpha_{ys},$$
$$\Delta V_{t2,ys} = (b/2 - e_2)K_{t0}\Delta\alpha_{ys} \tag{51}$$

The rotation equilibrium equation of the panels about $O_1$ and $O_2$ are

$$\Delta P_{ys}h + \Delta M_{\text{in}} - \Delta H_{\text{in}} \cdot h/2 - \Delta V_{h1,ys} \cdot b/2 = 0 \tag{52}$$

$$-\Delta M_{\text{in}} + \Delta H_{\text{in}} \cdot h/2 - \Delta V_s \cdot b - \Delta V_{h2,ys} \cdot b/2 = 0 \tag{53}$$

By adding Eqs. (52) and (53), the lateral pushing force that will yield the shear spring can be written

$$\Delta P_{ys} = K_h(e_2 + e_1) \cdot \alpha_{ys} \cdot \frac{b/h}{2} + [F_s - K_s b\alpha_{\text{up}}]b/h \tag{54}$$

## Appendix II. Formula for Six Stages of Coupled Rocking Wall Behavior

Stage 1: Decompression of the wall corner will occur when the rotation angle equals

$$\alpha_{\text{up}} = (W + V_{h0})/K_{t0}/b \tag{55}$$

and the lateral resistance equals

$$(W + V_{h0}) \cdot b/h \tag{56}$$

Stage 2: At yielding of the shear connectors, the incremental rotation angle is

$$\Delta\alpha_{ys} = [F_s/K_s/b - \alpha_{\text{up}}] \cdot [1 + 2K_s/(K_{t0} + K_h)] \tag{57}$$

and the incremental lateral resistance is

$$\frac{b^2 K_h K_{t0}}{2h(K_h + K_{t0})}\Delta\alpha_{ys} + [F_s - K_s b\alpha_{\text{up}}]b/h \tag{58}$$

Stage 3: At crushing of the right panel corner, the incremental rotation angle is

$$\Delta\alpha_{yt2} = \frac{F_t - W - V_{h0} - \Delta V_{t2,ys}}{(b/2 - e_2')K_{t0}} \tag{59}$$

and the incremental lateral resistance is

$$\frac{bK_h\Delta\alpha_{yt2}(e_1' + e_2')}{2h} \tag{60}$$

Stage 4: At crushing of the left panel corner, the incremental rotation angle is

$$\Delta\alpha_{yt1} = \frac{F_t - (W + \Delta V_{t1,ys} + \Delta V_{t1,yt2})}{(b/2 - e_1')K_{t0}} \tag{61}$$

and the incremental lateral resistance is

$$\frac{bK_h\Delta\alpha_{yt1}(e_1' + e_2'')}{2h} \tag{62}$$

Stage 5: At yielding of the left panel hold-down element, the incremental rotation angle is

$$\Delta\alpha_{yh1} = \frac{F_h/K_h - D_{h1,yt1}}{e_1''} \tag{63}$$

and the incremental lateral resistance is

$$\frac{bK_h\Delta\alpha_{yh1}(e_1'' + e_2'')}{2h} \tag{64}$$

Stage 6: At yielding of the right panel hold-down element, the incremental rotation angle is

$$\Delta\alpha_{yh2} = \frac{F_h/K_h - D_{h2,yh1}}{e_2''} \tag{65}$$

and the incremental lateral resistance is

$$\frac{bK_h\Delta\alpha_{yh2}(b/2 + e_2'')}{2h} \tag{66}$$

## Acknowledgments

This research project is supported by the National Science Foundation through a number of collaborative awards, including CMMI 1636164, CMMI 1634204, CMMI 1635363, CMMI 1635227, CMMI 1635156, CMMI 1634628. The use of the NHERI experimental facility is supported by the National Science Foundation's Natural Hazards Engineering Research Infrastructure Program. The authors also acknowledge support for the two-story shake table testing program from industry partners including Katerra, Simpson Strong-Tie, Forest Products Laboratory, Softwood Lumber Board, DR Johnson Lumber, and the City of Springfield, Oregon. The opinions presented here are solely those of the authors. The authors also acknowledge individual industry collaborators and students who worked on this project, including Reid Zimmerman, Jace Furley, Sarah Wichman, Leonardo Rodrigues, Brian DeMeza, Gabriele Tamagnone, Daniel Griesenauer, Ethan Judy, Steven Kordziel, Aleesha Busch, Ali Hansan, Joycelyn Ng, Monica Y. Liu, Ata Mohseni, and Da Huang. The authors also acknowledge the research collaboration on the Tall Wood project from James Ricles and Richard Sause at Lehigh University and Keri Ryan at the University of Nevada Reno; and finally, the help provided by the management and site staff of NHERI@UCSD.

## Notation

*The following symbols are used in this paper:*

$b$, $h$, and $t$ = width, height, and thickness, respectively, of each panel;
$D$ = elongation of springs;
$e_1$ and $e_2$ = rotation center distance on left panel on left and right panel, respectively, during Phase 2;
$e_1'$ = rotation center distance on left panel during Phases 3 and 4;

$e_2'$ = rotation center distance on left panel on right panel during Phase 3;

$e_1''$ = rotation center distance on left panel on left panel during Phase 5;

$e_2''$ = rotation center distance on left panel on right panel during Phases 4–6;

$F_h$ = yielding strength of hold-down spring;

$F_s$ = yielding strength of shear spring;

$F_t$ = yielding strength of toe spring;

$K_h$ = stiffness of hold-down spring;

$K_s$ = stiffness of shear connector before yielding;

$K_{t0}$ = initial stiffness of toe before yielding;

$K_{t1}$ = postyielding stiffness of toe;

$U$ = lateral displacement on wall top;

$V_{h0}$ = prestressing hold-down force;

$V_{h1}$, $V_{h2}$ = left and right hold-down force (excluding prestress load);

$V_s$ = shear force of interpanel connector;

$V_{t1}$ and $V_{t2}$ = left and right toe force, respectively;

$W$ = self-weight of one panel;

$\alpha$ = rotation angle of panel; and

$\Delta X$ = increment of $X$ with respect to former phase.

### Subscripts

up = decompression (Phase 1);

$ys$ = yielding of shear spring (Phase 2);

$yt2$ = yielding of the toe on right panel (Phase 3);

$yt1$ = yielding of the toe on left panel (Phase 4);

$yh1$ = yielding of left hold-down (Phase 5); and

$yh2$ = yielding of right hold-down (Phase 6).

## References


Akbas, T., et al. 2017. "Analytical and experimental lateral-load response of self-centering posttensioned CLT walls." *J. Struct. Eng.* 143 (6): 04017019. https://doi.org/10.1061/(ASCE)ST.1943-541X.0001733.

Belleri, A., M. J. Schoettler, J. I. Restrepo, and R. B. Fleishman. 2014. "Dynamic behavior of rocking and hybrid cantilever walls in a precast concrete building." *ACI Struct. J.* 111 (3): 661–672. https://doi.org/10.14359/51686778.

Caughey, T. K. 1963. "Equivalent linearization techniques." *J. Acoust. Soc. Am.* 35 (11): 1706–1711. https://doi.org/10.1121/1.1918794.

Computers and Structures. 2006. *Integrated finite element analysis and design of structures basic analysis reference manual*. Berkeley, CA: Computers and Structures.

Deierlein, G., H. Krawinkler, X. Ma, M. Eatherton, J. Hajjar, T. Takeuchi, K. Kasai, and M. Midorikawa. 2011. "Earthquake resilient steel braced frames with controlled rocking and energy dissipating fuses." *Steel Constr.* 4 (3): 171–175. https://doi.org/10.1002/stco.201110023.

Ganey, R., et al. 2017. "Experimental investigation of self-centering cross-laminated timber walls." *J. Struct. Eng.* 143 (10): 04017135. https://doi.org/10.1061/(ASCE)ST.1943-541X.0001877.

Loo, W. Y., C. Kun, P. Quenneville, and N. Chouw. 2014. "Experimental testing of a rocking timber shear wall with slip-friction connectors." *Earthquake Eng. Struct. Dyn.* 43 (11): 1621–1639. https://doi.org/10.1002/eqe.2413.

Pei, S., et al. 2017. "Development and full-scale validation of resilience-based seismic design of tall wood buildings: The NHERI Tallwood Project." In *Proc., New Zealand Society for Earthquake Engineering Annual Conf.* Wellington, New Zealand.

Pei, S., J. W. van de Lindt, and M. Popovski. 2013. "Approximate R-Factor for cross laminated timber walls in multi-story buildings." *J. Archit. Eng.* 19 (4): 245–255. https://doi.org/10.1061/(ASCE)AE.1943-5568.0000117.

Smith, T., F. Ludwig, S. Pampanin, M. Fragiacomo, A. Buchanan, B. Deam, and A. Palermo. 2007. "Seismic response of hybrid-LVL coupled walls under quasi-static and pseudo-dynamic testing." In Vol. 1 of *Proc., New Zealand Society for Earthquake Engineering Conf.*, 1–8. Palmerston North, New Zealand.

Wada, A., Z. Qu, H. Ito, S. Motoyui, H. Sakata, and K. Kasai. 2010. "Seismic retrofit using rocking walls and steel dampers." In *Improving the seismic performance of existing buildings and other structures*, 1010–1021.

# Queries

1. Please provide the ASCE Membership Grades for the authors who are members.

2. Please provide stree address for the author "H. Blomgren and J. Powers" in affiliation footnotes.

3. [ASCE Open Access: Authors may choose to publish their papers through ASCE Open Access, making the paper freely available to all readers via the ASCE Library website. ASCE Open Access papers will be published under the Creative Commons-Attribution Only (CC-BY) License. The fee for this service is $1750, and must be paid prior to publication. If you indicate Yes, you will receive a follow-up message with payment instructions. If you indicate No, your paper will be published in the typical subscribed-access section of the Journal.]

4. Please check the hierarchy of section heading levels.

5. The citation (Andrea et al. 2014) mentioned in this sentence is not present in the References list. Please provide the full details and we will insert it in the References list and link it to this citation.

6. Please check all figures, figure citations, and figure captions to ensure they match and are in the correct order.

7. Please specify “Appendix I” or “Appendix II”.

8. ASCE style for fences in math is in the order {[()]}. Please check to ensure all math conforms to this ASCE style.

9. Please confirm the change from “rotate center” to “center of rotation”.

10. ASCE style does not number sections. Please verify that the section reference is correct.

11. “distance on left panel on left and right panel” is unclear. Please rewrite this sentence to clarify its meaning.

12. “distance on left panel on right panel” is unclear. Please rewrite this sentence to clarify its meaning.

13. “distance on left panel on left panel” is unclear. Please rewrite this sentence to clarify its meaning.

14. “distance on left panel on right panel” is unclear. Please rewrite this sentence to clarify its meaning.

15. This reference Belleri et al. (2014) is not mentioned anywhere in the text. ASCE style requires that entries in the References list must be cited at least once within the paper. Please indicate a place in the text, tables, or figures where we may insert a citation or indicate if the entry should be deleted from the References list.

16. Please provide the publisher or sponsor name and location (not the conference location) for reference Pei et al. (2017).

17. Please provide the publisher or sponsor name and location (not the conference location) for reference Smith et al. (2007).

18. Please provide publisher name and location for reference Wada et al. (2010).